RSC Advances

ROYAL SOCIETY OF CHEMISTRY

PAPER

View Article Online
View Journal | View Issue

Cite this: *RSC Adv.*, 2026, **16**, 10346

Fabrication of potential environmentally friendly 3D printing biocomposite filament based on poly(lactic acid) and cellulose fibers from agricultural waste

Nguyen Chi Thanh, *[a] Pham Duc Thinh,[a] Bui Phuong Dong,[a] Tran Hai Cat[a] and Nguyen Thanh Huy [bc]

This study focuses on the fabrication of biocomposites based on poly(lactic acid) (PLA) and cellulose fibers (CMF) extracted from corn cob agricultural waste using a simple alkaline hydrogen peroxide (HPK) treatment. The HPK process was optimized by varying the ratio of weight of raw material and volume of used chemicals (wt/V), reaction temperature, and reaction time. The extracted cellulose fibers were used as reinforcing agents in the PLA matrix to improve the mechanical properties of the biocomposites. To enhance compatibility and interfacial adhesion between the cellulose fibers and the polymer matrix, the fiber surface was chemically modified using rice bran oil (RBO), an environmentally friendly modification agent. Scanning electron microscopy (SEM) and Fourier-transform infrared spectroscopy (FTIR) analyses confirmed the effective removal of surface impurities, hemicellulose, and lignin from the corn cobs after HPK treatment. X-ray diffraction (XRD) results showed that the treated cellulose fibers exhibited a higher crystallinity index than the raw material, while thermogravimetric analysis (TGA) demonstrated improved thermal stability of the cellulose fibers. Differential scanning calorimetry (DSC) indicated that the incorporation of RBO-modified cellulose fibers enhanced the crystallization rate of PLA, and rheological measurements revealed higher viscosity of PLA/RBO1 biocomposites compared to neat PLA across the entire shear rate range. Tensile test results demonstrated that biocomposites containing RBO-modified cellulose fibers exhibited significantly improved mechanical properties, with the composite containing 1 wt% CMF achieving the highest performance. Furthermore, PLA/RBO1 composite filaments showed good printability *via* fused deposition modeling (FDM), highlighting their potential as environmentally friendly materials for 3D printing applications.

Received 15th December 2025
Accepted 11th February 2026

DOI: 10.1039/d5ra09705c

rsc.li/rsc-advances

Introduction

In the context of increasing environmental pollution and the urgent need for sustainable materials, the development of bio-based composites from renewable resources has garnered significant attention.[1] The extraction and utilization of non-renewable resources not only deplete natural reserves but also exacerbate plastic waste and environmental pollution issues. This scenario highlights the critical demand for scientists and industries to explore and develop novel materials derived from renewable, eco-friendly, and biodegradable sources.[2]

Vietnam is an agricultural country with a substantial amount of agricultural waste generated annually.[3] Among the by-products, corn cob-a residue from corn processing has attracted growing interest due to its high recyclability and wide-ranging applications.[4] The utilization of corn cobs not only reduces agricultural waste but also adds economic value to the circular economy. The primary composition of corn cobs includes cellulose (30–50%), hemicellulose (30–40%), and lignin (5–10%). Due to their high cellulose content, corn cobs serve as an excellent raw material for developing environmentally friendly bio-based materials.[5]

Cellulose extracted from lignocellulosic biomass was obtained at the nano or micro scale using various methods, including chemical, biological, and mechanical processes, to remove hemicellulose, lignin, pectin, and other amorphous components found in corn cobs.[6] Chemical methods commonly used for cellulose extraction involved acid and alkaline

[a]*Faculty of Applied Sciences, Ho Chi Minh City University of Technology and Engineering, 01 Vo Van Ngan Street, Thu Duc Ward, Ho Chi Minh City, Vietnam. E-mail: thanhnc@hcmute.edu.vn; 20130064@student.hcmute.edu.vn; 20130020@student.hcmute.edu.vn; catth@hcmute.edu.vn*

[b]*Department of Polymer Materials, Faculty of Materials Technology, Ho Chi Minh City University of Technology (HCMUT), 268 Ly Thuong Kiet Street, Dien Hong Ward, Ho Chi Minh City, Vietnam. E-mail: nthuy.sdh241@hcmut.edu.vn*

[c]*Vietnam National University Ho Chi Minh City, Thu Duc Ward, Ho Chi Minh City, Vietnam*

treatments. Alkaline solutions such as NaOH, KOH, and $Ca(OH)_2$ were typically employed to remove hemicellulose and lignin from the chemical structure of corn cobs, while inorganic acids (H_2SO_4, HNO_3,…) and organic acids (acetic acid, formic acid,…) were used to isolate cellulose.[7] However, chemical treatments generated byproducts that contributed to environmental pollution and degraded the quality of the extracted cellulose. Biological methods, which were considered environmentally friendly, eliminated the need for hazardous chemicals. These methods utilized microorganisms and enzymes to degrade hemicellulose and lignin, yielding high-purity cellulose.[8] Despite their advantages-such as sustainability and minimal chemical consumption-biological methods had certain limitations, including high costs, slow processing times, and challenges in process control. Meanwhile, mechanical methods relied on strong physical forces to separate cellulose fibers. Common techniques included grinding, high-pressure homogenization, and ultrasonication.[9] However, mechanical processing was highly energy-intensive and was often combined with other methods to enhance extraction efficiency. Each method had its own advantages and limitations, and the selection of an appropriate approach depended on the intended application. In this study, chemical treatment using an H_2O_2/NaOH system was applied to extract cellulose from agricultural waste, specifically corn cobs.

As a natural polymer, cellulose fibers possess significant advantages such as non-toxicity, biodegradability, renewability, and biocompatibility, making this natural fiber an attractive alternative to synthetic polymers in various applications, including food, pharmaceuticals, cosmetics, and composite materials.[10,11]

Poly(lactic acid) (PLA) is a bio-based polymer synthesized from renewable feedstocks such as corn starch and sugarcane.[2] With the chemical formula $(C_3H_4O_2)_n$, PLA belongs to the poly(α-hydroxy ester) group and features a helical molecular structure with orthorhombic unit cells, forming a tightly packed network.[12] This molecular structure significantly influences the physical properties of PLA, including its melting temperature (T_m) and glass transition temperature (T_g).[13,14] PLA is widely used due to its biodegradability, excellent biocompatibility, and ease of processing.[15] However, PLA exhibits several limitations, such as brittleness, low thermal stability, and poor crystallinity, which hinder its mechanical performance.[16] Incorporating cellulose fibers into the PLA matrix had been demonstrated as an effective approach to enhance mechanical strength, thermal stability, and crystallinity while maintaining the material's biodegradability.[17]

Reported studies explored the reinforcement of PLA-based composites using nanocrystalline cellulose (CNCs) extracted from corn cobs, which significantly improved the tensile strength and crystallinity index of polymer composite.[1] Furthermore, surface modification of cellulose fibers had been shown to enhance fiber-matrix interfacial adhesion, leading to superior mechanical properties in biocomposites.[18]

3D printing technology is revolutionizing industrial manufacturing due to its flexibility, high customization potential, and ability to minimize material waste.[19] However, most current 3D printing materials are synthetic polymers, which are non-biodegradable and significantly contribute to environmental pollution.[20] Therefore, the development of biodegradable and renewable 3D printing materials has emerged as a critical trend in sustainable manufacturing.[15,21]

Based on this premise, this study focused on the fabrication of PLA-based biocomposites reinforced with corn cobs-derived cellulose fibers, aiming to develop eco-friendly materials for 3D printing applications.[22,23] By optimizing cellulose extraction and surface modification processes, this research not only seeks to reduce environmental pollution but also addresses the growing demand for bio-based 3D printing materials, contributing to the advancement of a circular and sustainable economy.

Materials and methods

Materials

Corn cobs were collected from Giang Dien Commune, Trang Bom District, Dong Nai Province, Vietnam. Hydrogen peroxide (H_2O_2), sodium hydroxide (NaOH), and ethanol were obtained from Sigma-Aldrich. A commercial grade of PLA (PLA 4043D) was purchased from NatureWorks. Distilled water was supplied by the Material Technology Laboratory, Faculty of Applied Sciences, Ho Chi Minh City University of Technology and Education (HCMUTE).

Methods

Extraction of cellulose fibers from corn cobs using alkaline hydrogen peroxide (HPK) treatment. The collected corn cobs were sun-dried and ground into fine powder. The powder was sieved to obtain a uniform particle size and then dried in an oven at 70 °C for 24 h to remove residual moisture. Subsequently, 10 g of the dried corn cobs powder was placed in a laboratory flask and mixed with 150 mL of a 2% hydrogen peroxide (H_2O_2) solution. The pH of the mixture was adjusted to 11.5 using 5 M sodium hydroxide (NaOH). The mixture was then heated to 50 °C and continuously stirred using a magnetic stirrer for 4 h. Finally, the sample was filtered and washed until neutral pH was achieved, followed by drying at 50 °C for 24 h.

After the reaction, the mixture was filtered to separate the solid residue (primarily cellulose) from the liquid phase containing degraded components. The solid residue was washed thoroughly with distilled water until a neutral pH was achieved to remove any remaining impurities. The reaction conditions, such as the raw material-to-chemical solution ratio, reaction temperature, and reaction time, were respectively presented in Tables 1–3.

Surface modification of cellulose fibers using rice bran oil (RBO). To enhance the interfacial compatibility between cellulose fibers and the PLA matrix, the extracted CMF were subjected to surface modification using rice bran oil (RBO), a bio-based and environmentally friendly modifier. The chemical modification process aimed to reduce the hydrophilicity of cellulose fibers while improving their dispersion within the polymer matrix as well as the interfacial adhesion between two

Table 1 Experimental conditions for examining the influence of the raw material-to-chemical solution ratio

Reaction parameters	CMF-TL1	CMF-TL2	CMF-TL3
Raw material-to-chemical solution ratio[a] (wt/V)	**1/10**	**1/15**	**1/20**
Reaction time (hours)	4	4	4
Reaction temperature (°C)	50	50	50

[a] This table presents the experimental conditions for testing the influence of the raw material-to-chemical solution ratio on the extraction of cellulose from corn cobs. The ratios of 1/10, 1/15, and 1/20 (wt/V) were tested under a constant reaction time of 4 hours at 50 °C.

Table 2 Experimental conditions for examining the effect of reaction temperature

Reaction parameters	CMF-T1	CMF-T2	CMF-T3
Raw material-to-chemical solution ratio (wt/V)	1/10	1/10	1/10
Reaction time (hours)	4	4	4
Reaction temperature[a] (°C)	**50**	**60**	**70**

[a] The table shows the experimental conditions used to examine the effect of varying reaction temperatures on the extraction process. The reaction temperature was varied at 50 °C, 60 °C, and 70 °C, while the raw material-to-chemical ratio was maintained at 1/10 (wt/V) for 4 hours.

Table 3 Experimental conditions for investigating the effect of reaction time

Reaction parameters	CMF-T1	CMF-T2	CMF-T3
Raw material-to-chemical solution ratio (wt/V)	1/10	1/10	1/10
Reaction time[a] (hours)	**3**	**4**	**5**
Reaction temperature (°C)	50	50	50

[a] This table outlines the experimental conditions used to investigate the influence of reaction time on the cellulose extraction process from corn cobs treated with hydrogen peroxide-alkaline (HPK). The experiment was conducted at three different reaction times (3, 4, and 5 hours) under a constant raw material-to-chemical ratio of 1/10 (wt/V) and reaction temperature of 50 °C.

phases. Firstly, the extracted cellulose fibers were dried at 50 °C for 24 hours to remove residual moisture before chemical modification treatment. A solution of 5 wt% RBO in ethanol was prepared under constant stirring to ensure homogeneous dispersion of the oil. After that, the dried cellulose fibers were immersed in the prepared RBO-ethanol solution and subjected

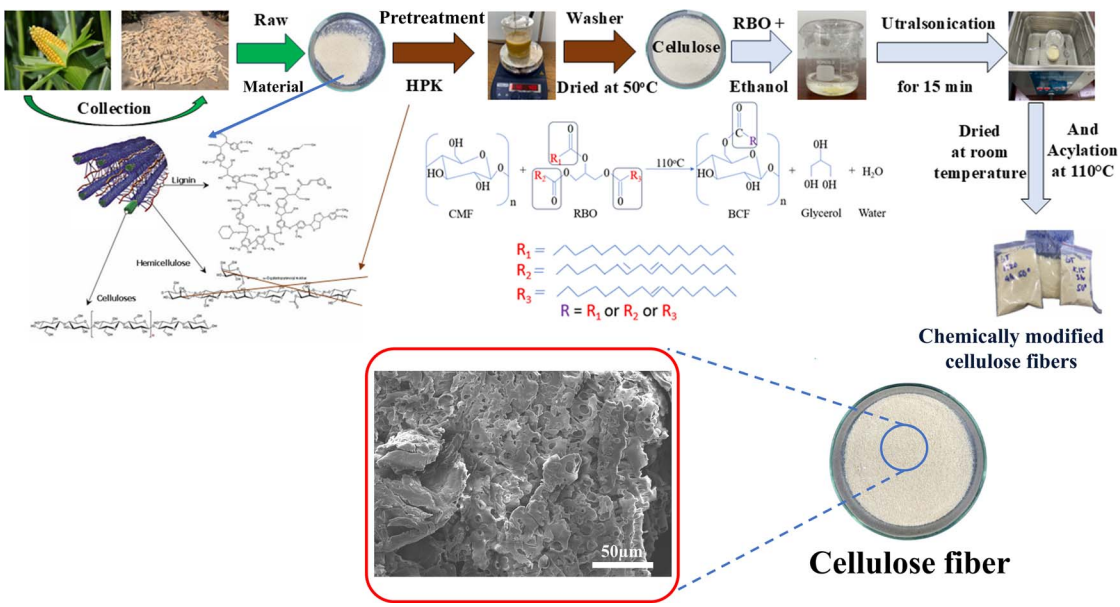

Fig. 1 Extraction process and chemical modification of cellulose fibers.

Table 4 Composition of biocomposites based on PLA and extracted cellulose fibers

Symbol	PLA (wt%)	Unmodified CMF (wt%)	RBO-chemically modified CMF (wt%)
PLA	100	—	—
PLA/CMF1	99.0	1.0	—
PLA/CMF5	95.0	5.0	—
PLA/CMF10	90.0	10.0	—
PLA/RBO1	99.0	—	1.0
PLA/RBO5	95.0	—	5.0
PLA/RBO10	90.0	—	10.0

to ultrasonication for 15 minutes to facilitate the penetration of RBO molecules into the fiber structure. Finally, the fibers were dried at room temperature and further subjected to thermal acylation at 110 °C for 2 hours, promoting the esterification reaction between RBO and the hydroxyl groups of cellulose. The cellulose fibers extraction and surface chemical modification processes were described in Fig. 1.

Preparation of biocomposites based on extracted cellulose fibers and PLA. The biocomposites between unmodified and chemically modified cellulose fibers and poly(lactic acid) were fabricated by melt mixing method using an internal mixer (Haake Rheomix, 3000p) at a temperature of 170 °C. The ratio of each component of composites is shown in Table 4. The mixing time and mixing speed were kept at 10 min and 60 rpm, respectively. The fabrication of PLA/cellulose fibers biocomposite consists of two main stages: drying of materials and mixing of components.

PLA and cellulose fibers were dried in an oven at 70 °C for 3 hours to remove residual moisture. This step ensures material quality and stability during melting mixing. Subsequently, the determined amounts of dried PLA and cellulose fiber were premixed using a mechanical mixer. All compositions of biocomposites were charged into the mixing chamber at the same time. The fabrication process of the biocomposites based on the extracted cellulose fibers and PLA was illustrated in Fig. 2.

Fabrication of biocomposite filament based on extracted cellulose fibers and PLA. The biocomposite filament fabrication process was carried out using extrusion technique. Filament of PLA/CMF biocomposites was prepared by Felfil EVO 3D printing filament extruder. The filament fabrication process was conducted at the Materials Technology Laboratory, Faculty of Applied Sciences, Ho Chi Minh City University of Technology and Education. In this experiment, PLA and 1 wt% of chemically modified cellulose fibers were used to produce filament for 3D printing. Before conducting the extrusion process, PLA pellets and chemically modified cellulose fibers were dried at 70 °C for 2 hours to remove excess moisture, improving processability and filament quality. Then, the dried PLA and cellulose fibers were thoroughly pre-mixed before feeding the materials into the extruder. The filament fabrication process was carried out at 190 °C with screw speed set to 6 level. Under heat and pressure, the melted material was extruded through the die, forming a continuous filament with a relatively uniform diameter. The extruded filament was cooled, collected, and wound onto spools. The fabrication process of biocomposite filament based on extracted cellulose fibers and PLA was illustrated in Fig. S1 of the SI.

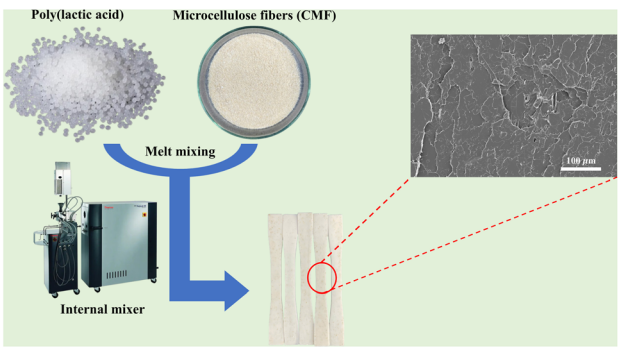

Fig. 2 Schematic diagram of the experimental process for fabricating PLA/CMF biocomposites.

Characterization analysis

Crystalline structure characterization. X-ray diffraction (XRD) technique was used to determine the crystalline structure of corn cobs agricultural waste, extracted cellulose fibers, and PLA-based biocomposite materials. Based on the position of the diffraction peaks and the intensity of the diffraction peaks, the crystalline structure as well as the relative crystallinity of the samples were evaluated. In this characterization, corn cobs, cellulose fibers, and biocomposite materials were analyzed using an EMPYREAN X-ray diffractometer from PANalytical (Netherlands) at the University of Finance and Marketing in Ho Chi Minh City, Vietnam. All measurements were performed over an 2θ range from 5° to 80°, using Cu Kα radiation ($\lambda = 1.54056$ Å) at 40 kV and 45 mA. The crystallinity index was quantitatively calculated according to the following eqn (1):

$$\mathrm{CrI}(\%) = \frac{I_{200} - I_{\mathrm{am}}}{I_{200}} \times 100 \quad (1)$$

The crystallinity index (CrI) represents the relative degree of crystallinity within the material. The intensity I_{200} corresponds to the maximum diffraction intensity of the 002 lattice plane, typically observed between $2\theta = 22°$ and 23°, while I_{am} represents the minimum intensity, located between the 002 and 101 diffraction peaks, generally within the range of $2\theta = 18°$ to 19°. It is assumed that I_{am} primarily accounts for the amorphous contribution with minimal crystalline influence, whereas I_{200} encompasses both crystalline and amorphous regions.[24]

The crystallinity index (CrI) of PLA and PLA/CMF composites was calculated according to eqn (2).

$$\mathrm{CrI}_{\mathrm{PLA/CMF}}(\%) = \frac{\sum A_{\mathrm{crystalline}}}{\sum A_{\mathrm{crystalline}} + \sum A_{\mathrm{amorphous}}} \times 100 \quad (2)$$

where $A_{\mathrm{crystalline}}$ and $A_{\mathrm{amorphous}}$ are the areas under the diffraction peaks corresponding to the crystalline and amorphous regions, respectively.[25]

Thermal properties analysis. The thermal stability of corn cobs and extracted cellulose fibers was determined using a TGA/DSC 3+ thermal analyzer from Mettler Toledo (Switzerland) at the Institute of Applied Materials Science, Ho Chi Minh City, Vietnam. The samples were heated from 25 °C to 600 °C at a heating rate of 10 °C min^{-1} under a nitrogen flow of 20 mL min^{-1}.

Thermal properties of PLA and PLA/CMF biocomposites were characterized by differential scanning calorimetry (DSC) (model: DSC204F1 Phoenix) technique. The measurements were conducted by heating the specimens from 40 to 200 °C at a heating rate of 5 °C min^{-1} for the first heating scan to remove thermal history. After keeping the specimens at 200 °C for 5 min, they were cooled to 40 °C at 5 °C min^{-1}. Subsequently, the samples were heated again to 200 °C at 5 °C min^{-1} for the second heating scan.

Surface morphology analysis by SEM. Scanning Electron Microscopy (SEM) technique was used to examine the microstructure and surface morphology of cellulose fibers and biocomposites. The analysis was conducted using a SEM (FE-SEM, Hitachi S4800 equipped with EDS system, Oxford). During sample preparation, the specimens were mounted onto metal stubs using carbon tape. Prior to observation, all samples were coated with a thin layer of gold to ensure electrical conductivity. All SEM images were collected under an acceleration voltage of 15 kV.

Cellulose recovery yield. The cellulose recovery yield was calculated based on mass percentage according to eqn (3):

$$\text{Recovery yield}(\%) = \frac{m_1}{m_0} \times 100 \quad (3)$$

where m_0 is the mass of the raw material (g) and m_1 is the mass of the sample after the extraction process (g).

Chemical structure analysis. The chemical structure of corn cobs and cellulose fibers was analyzed using a Fourier Transform Infrared Spectrometer (FTIR), NICOLET 6700-Therm (USA). The samples were measured within the wavenumber range of 400–4000 cm^{-1}, with a resolution of 4 cm^{-1} and 64 scans.

Mechanical properties analysis of PLA/CMF biocomposites. The mechanical properties of the fabricated biocomposite materials were evaluated by measuring the tensile strength of the biocomposites reinforced with different cellulose fiber contents. The measurements were performed using a SHIMADZU AGS-X testing machine. The tensile strength of the materials was determined according to ASTM D638 standard, with a testing speed of 5 mm min^{-1}.

Rheological properties of PLA/CMF biocomposites. Rheological properties of PLA and PLA/CMF biocomposites were studied by measuring shear viscosities at various shear rates using Rheograph 20 rheometer (model RG 120) at 170 °C. Melt flow index (MFI) of PLA and PLA/CMF biocomposites was characterized using a melt flow indexer (Kayeness, 4004). All measurements were conducted according to the standard of ASTM D1238 at 170 °C with a load of 2.16 kg. The extrudate in gram per 10 min was presented.

Dimensional accuracy. The dimensional accuracy of the 3D-printed specimens was evaluated based on the designed model. The length, width, and thickness of the printed samples were measured five times using a digital caliper (MITUTOYO 500-181-30, measuring range: 0–150 mm, resolution: 0.01 mm). The dimensional deviation (%) was calculated using the following eqn (4):[26]

$$\text{Deviation}(\%) = \frac{a-b}{a} \times 100 \quad (4)$$

where a is the designed dimension and b is the actual dimension of the printed sample.

Statistical analysis. Analysis of variance (ANOVA) followed by Tukey's post hoc test was performed using IBM SPSS Statistics 20 for Windows. All experiments were carried out in triplicate ($n = 3$) and evaluated by one-way ANOVA at a 95% confidence level, where p-values < 0.05 were considered statistically significant.

Results and discussion

Crystalline structure of corn cobs and extracted cellulose fibers

Effect of the raw material-to-chemical solution ratio. As observed in Fig. 3 and Table 5, all samples exhibited diffraction peaks at 18.5°, 22.5°, and 34.6° corresponding to the diffraction planes 101, 002, and 040, which are characteristic of the crystalline structure of cellulose fibers. This indicated that the HPK treatment process did not destroy the chemical structure of cellulose.[27]

Compared to the CC sample, all CMF-TL treated samples exhibited higher crystallinity index, indicating that the HPK treatment effectively removed amorphous components such as hemicellulose, lignin, and non-cellulose compounds. Furthermore, as shown in Table 5, decreasing the ratio of raw material

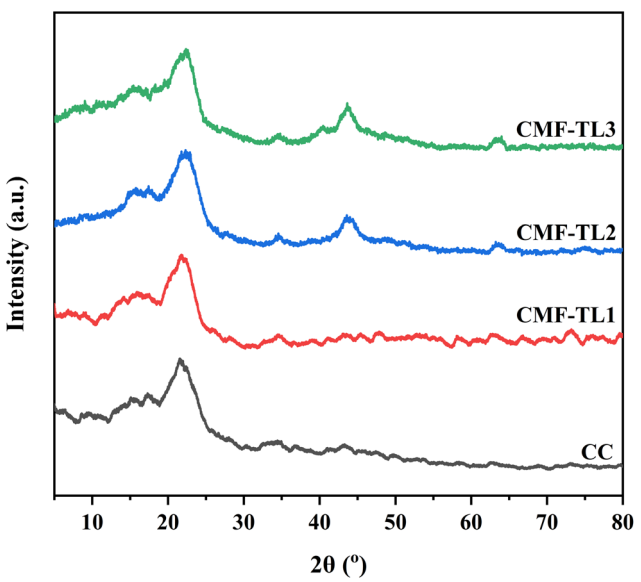

Fig. 3 XRD patterns of the untreated corn cobs sample (CC) and the hydrogen peroxide alkaline treated samples with different raw material-to-chemical solution ratios (CMF-TL1, CMF-TL2, CMF-TL3).

Table 5 Crystallinity index of the untreated corn cobs sample (CC) and the hydrogen peroxide alkaline treated samples with different raw material-to-chemical solution ratios (CMF-TL), calculated using eqn (1) [a]

Sample	Crystallinity index (%)
CC	35.42 ± 1.40
CMF-TL1	39.03 ± 0.98[a]
CMF-TL2	38.56 ± 0.76[a]
CMF-TL3	38.93 ± 1.02[a]

[a] a: Do not show statistically significant differences among the samples.

to chemical solution from 1/10 (wt/V) to 1/15 (wt/V) resulted in a decrease in crystallinity index from 40.48 ± 0.52% to 38.56 ± 0.76%. When the ratio was changed from 1/15 (wt/V) to 1/20 (wt/V), a slight increase in crystallinity was observed. The higher chemical volume contributed to the removal of impurities like hemicellulose, lignin, and other non-cellulosic substances, however, it may also have slightly reduced the cellulose crystallinity due to partial hydrolysis.[28] Among the investigated raw material-to-H_2O_2 solution ratios, the 1/10 (wt/V) ratio exhibited a higher crystallinity index than the 1/15 (wt/V) and 1/20 (wt/V) ratios, although the differences were not statistically significant, as shown by the ANOVA analysis in Table S1 of the SI. Therefore, the 1/10 (wt/V) ratio was selected for subsequent experiments to optimize the process efficiency.

Effect of reaction temperature. In the study of the effect of reaction temperature on the crystallinity of cellulose fibers extracted from corn cobs, the reaction was conducted for 4 hours at an optimal raw material-to-chemical ratio of 1/10 (wt/V), with varying reaction temperatures: 50 °C (CMF-T1), 60 °C (CMF-T2), and 70 °C (CMF-T3).

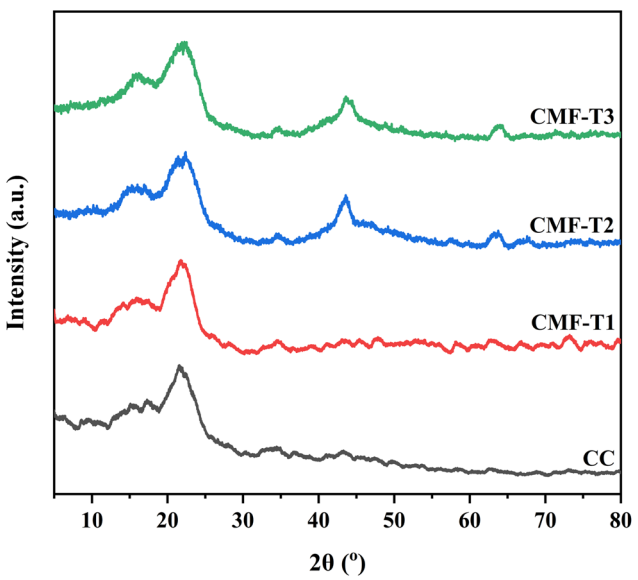

Fig. 4 XRD patterns of the untreated corn cobs sample (CC) and the hydrogen peroxide alkaline treated samples with different reaction temperatures (CMF-T1, CMF-T2, CMF-T3).

As observed from Fig. 4, the diffraction peaks remain characteristic at 18.5°, 22.5°, and 34.6°, corresponding to the diffraction planes 101, 002, and 040, respectively. Compared to the CC sample, all CMF-T samples showed higher crystallinity index.

Table 6 indicates that the sample treated at 50 °C has the highest crystallinity index compared to other samples. From the results in Fig. 4 and Table 6, it is evident that as the reaction temperature increases from 50 °C to 70 °C, the crystallinity index tends to decrease. In addition, ANOVA analysis showed that the reaction temperature significantly affected the crystallinity index of cellulose ($P < 0.05$), as presented in Table S2 of the SI. This is because at higher reaction temperatures, hydrolysis occurred, which may remove partially the crystalline regions, leading to a reduction in the crystallinity of cellulose.

Since the CMF-T1 sample treated at 50 °C exhibited the highest crystallinity index, it was selected as the optimal reaction temperature for further investigation of subsequent reaction condition parameter.

Effect of reaction time. In this experiment, the treatment reaction was carried out at the optimal temperature of 50 °C and an optimal raw material-to-chemical ratio of 1/10 (wt/V) for reaction times of 3 hours (CMF-T1), 4 hours (CMF-T2), and 5 hours (CMF-T3).

From the results in Fig. 5 and Table 7, it is evident that after treatment, the crystallinity of the CMF-T samples increased compared to the untreated CC sample. As can be seen from Fig. 5 and Table 7, the sample treated for 4 hours (CMF-T2) presented the highest crystallinity (40.48 ± 0.52%), indicating that this reaction time was effective for removing the amorphous components, allowing cellulose molecules to reorganize into a stable crystalline structure.[29] Additionally, the CMF-T3 samples showed a slight decrease in crystallinity compared to CMF-T2 sample, suggesting that too long treatment time may adversely affect the crystallinity of cellulose upon HPK treatment. Furthermore, ANOVA analysis indicated that the reaction time significantly affected the crystallinity index of the extracted cellulose ($P < 0.05$), as shown in Table S3 of the SI. Therefore, the optimal reaction time for obtaining the best cellulose crystallinity is 4 hours.

Thermal stability of cellulose fibers

Effect of the raw material-to-chemical ratio. From the thermograms in Fig. 6a, it is observed that all samples exhibit three main stages of degradation. The first stage, between 60 °C and

Table 6 Crystallinity index of the CC and CMF-T samples, calculated using eqn (1) [a]

Sample	Crystallinity index (%)
CC	35.42 ± 1.40
CMF-T1	39.03 ± 0.98[a]
CMF-T2	35.42 ± 1.26[b]
CMF-T3	35.18 ± 0.53[b]

[a] a, b: Show statistically significant differences among the samples.

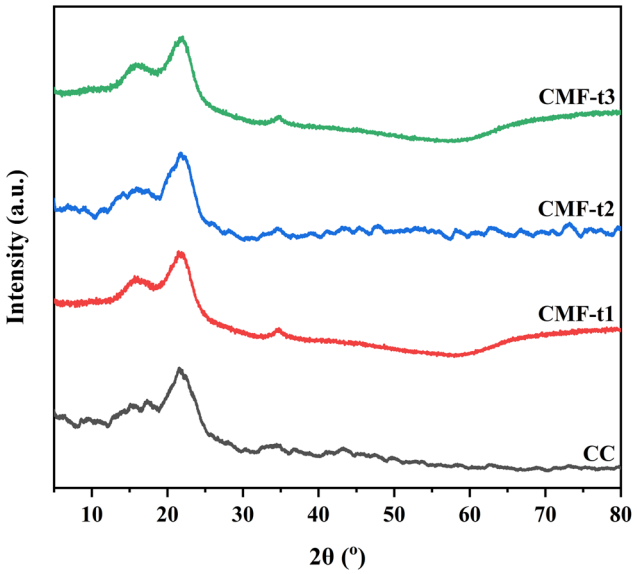

Fig. 5 XRD patterns of the untreated corn cobs sample (CC) and the hydrogen peroxide alkaline treated samples with different reaction times (CMF-T1, CMF-T2, CMF-T3).

Table 7 Crystallinity index of the CC and CMF-T samples, calculated using eqn (1) [a]

Sample	Crystallinity index (%)
CC	32.97 ± 0.80
CMF-T1	31.95 ± 0.58[b]
CMF-T2	39.03 ± 0.98[a]
CMF-T3	31.44 ± 1.03[b]

[a] a, b: Show statistically significant differences among the samples.

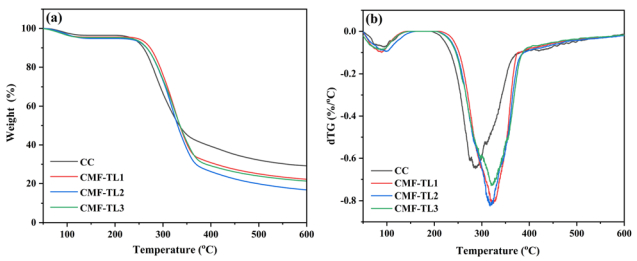

Fig. 6 (a) TGA, and (b) dTG curves of the CC sample and the CMF-TL1, CMF-TL2, and CMF-TL3 samples.

120 °C, shows a slight mass loss of 5–8%, primarily due to the evaporation of water content in the samples. The second stage, occurring between 250 °C and 350 °C, corresponds to the thermal degradation of hemicellulose and cellulose. The final stage, between 350 °C and 600 °C, is associated with the thermal degradation of lignin component.[30] The analysis results show that the CMF-TL1, CMF-TL2, and CMF-TL3 samples all have a higher onset degradation temperature compared to the CC sample. This indicates that the HPK treatment was effective in enhancing the thermal stability of the cellulose fibers.

Specifically, the dTG curves at Fig. 6b show that the CMF-TL1 sample exhibits the highest decomposition temperature, indicating the raw material-to-chemical ratio of 1/10 (wt/V) is optimal for the treatment. The higher thermal degradation temperatures observed in the CMF-TL samples compared to the CC sample can be attributed to the removal of a portion of hemicellulose and lignin after chemical treatment.

These results show that the ratio of raw material to chemical solution directly influenced on the thermal stability of the extracted cellulose fibers. Specifically, increasing the ratio from 1/10 (wt/V) to 1/20 (wt/V) resulted in a slight decrease in thermal stability of the obtained cellulose fibers.

Effect of reaction temperature. As observed from Fig. 7, the HPK treatment affected the thermal stability of the samples. Fig. 7 presents that the samples undergo multiple stages of thermal degradation, particularly in the temperature range of 200 °C to 400 °C. This indicates the presence of several components within the samples.

From the Fig. 7, it is evident that upon increasing the reaction temperature from 50 to 70 °C, the thermal stability of extracted cellulose fibers tended to decrease. Compared to raw corn cob sample, the obtained cellulose fibers had higher thermal stability. This result is ascribed to the effective removal of amorphous and non-cellulosic components upon chemical treatment.[31] The cellulose fibers extracted with reaction temperature of 50 °C demonstrated the best thermal stability.

Effect of reaction time. Fig. 8 show the TGA and dTG curves of the CC sample and cellulose fibers extracted with different times. As can be seen from Fig. 8 as reaction time increases from 3 to 5 hours, the thermal stability of cellulose fibers did not change significantly.

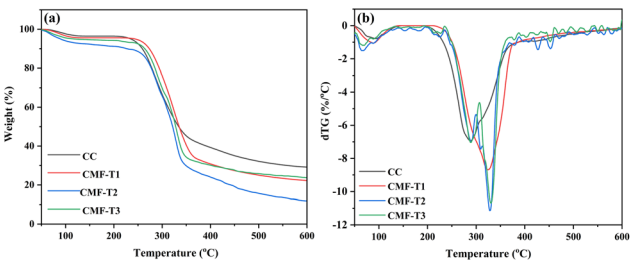

Fig. 7 (a) TGA, and (b) dTG curves of the CC sample and the CMF-T1, CMF-T2, and CMF-T3 samples.

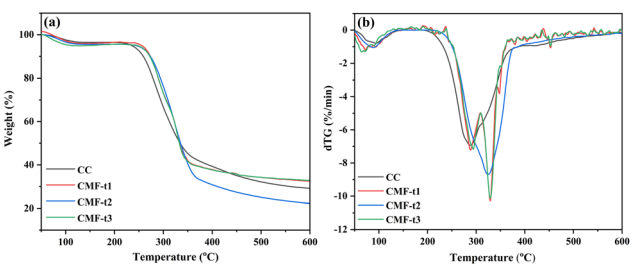

Fig. 8 (a) TGA, and (b) dTG curves of the CC sample and the CMF-T1, CMF-T2, and CMF-T3 samples.

Additionally, as observed from Fig. 8, the extracted cellulose fibers indicated the higher thermal stability compared to the raw CC sample. This confirms the effectiveness of the HPK treatment in improving the thermal stability of cellulose fibers.[32]

Chemical structure of corn cobs and extracted cellulose fibers

The FTIR spectra of raw corn cobs (CC) and cellulose fibers (CMF) was shown in Fig. 9. As observed, a broad band at 3400 cm^{-1} corresponding to the stretching vibrations of the –OH groups appeared in the FTIR spectrum of both raw corn cobs and cellulose fibers. This peak is characteristic of hydroxyl-containing compounds such as cellulose.[33] Besides that, the absorption peak at 2909 cm^{-1} attributed to the stretching vibrations of C–H bonds in methyl, methylene, or methine groups is presented in the FTIR spectrum of raw corn cobs and extracted cellulose fibers. The peak at 1043 cm^{-1} is associated with the C–O–C bonds in the chemical structure of cellulose. As shown in Fig. 9, both CC and CMF samples retain this characteristic peak. These results indicate that after chemical treatment, the chemical structure of cellulose remained intact.

However, compared to the FTIR spectrum of raw corn cobs, the FTIR spectrum of extracted cellulose fiber revealed a slight increase in the intensity of the peak at 3400 cm^{-1}. This demonstrates more free hydroxyl groups in the chemical structure of treated sample. Notably, there was a clear reduction in the intensity of the absorption peaks at 1732 cm^{-1} and 1510 cm^{-1} in the FTIR spectrum of cellulose fiber compared to that of raw corn cobs. These peaks are corresponded to the stretching vibrations of C=O and C=C (aromatic rings) bond, respectively. These bonds present in the chemical structure of hemicellulose and lignin component. This result indicates that the non-cellulosic components such as hemicellulose and lignin were effectively removed upon the HPK treatment.[34]

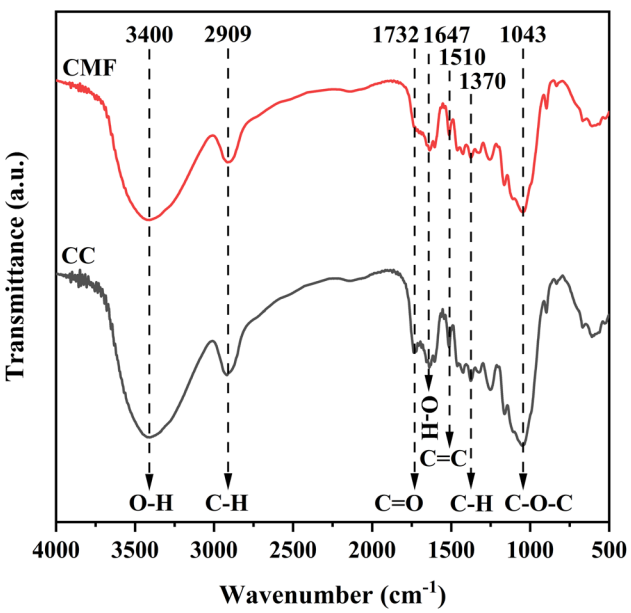

Fig. 9 FTIR spectra of the untreated corn cobs sample (CC) and the hydrogen peroxide alkaline treated sample (CMF).

Surface morphology of corn cobs and extracted cellulose fibers

Fig. 10 presented scanning electron microscopy (SEM) images of the untreated corn cob (CC) and the corn cob after HPK treatment (CMF). As shown in Fig. 10a, the untreated corn cob sample exhibited a rough and heterogeneous surface morphology, characterized by a layered structure in which cellulose fibers were tightly bound to amorphous components, mainly lignin and hemicellulose.[32,35] This structural feature was typical of untreated agricultural waste.[36] In contrast, the corn cob sample after HPK treatment exhibited pronounced morphological changes (Fig. 10b). The original layered structure was disrupted, and internal cellulose cavities became evident.[31] These changes were attributed to the effective removal of hemicellulose and lignin from the surface layers of the biomass, resulting in a smoother and more homogeneous surface.[37] This observation was consistent with previous studies reporting surface disruption and fiber exposure in corn cob and corn stalk residues after hydrogen peroxide-alkaline treatment.[38]

Cellulose recovery yield. The recovery yield of cellulose extracted under the optimal conditions (solid-to-liquid ratio of 1/10 wt/V, 50 °C, and 4 h), as calculated according to eqn (3), was 68.82 ± 3.92%.

Chemical structure of cellulose fibers after chemically modifying with RBO

The results in Fig. 11 showed that both FTIR spectra of CMF, and CMF/RBO exhibited characteristic peaks at 3400, 2909, 1370, 1043, and 897 cm^{-1}, corresponding to the structural groups of cellulose.[39] This confirmed that upon chemical modification treatment, the chemical structure of cellulose was intact. The broad band observed at 3400 cm^{-1} indicated a reduction in the number of hydroxyl (–OH) groups, suggesting that esterification occurred with the acyl groups of RBO in the CMF/RBO sample.[29] The absorption peaks in the region of 2800–3100 cm^{-1}, corresponding to the alkyl groups (2853 and 2924 cm^{-1}) and acyl groups (3006 cm^{-1}), significantly increased in the RBO-CMF sample. Additionally, compared to the FTIR spectrum of CMF sample, the FTIR spectrum of RBO-CMF sample presented the appearance of a new sharp peak at

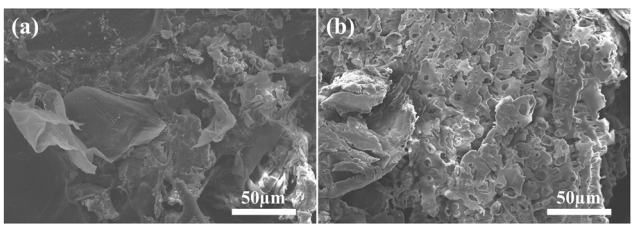

Fig. 10 SEM images of (a) raw corn cobs sample (CC) and (b) hydrogen peroxide-alkaline treated sample (CMF).

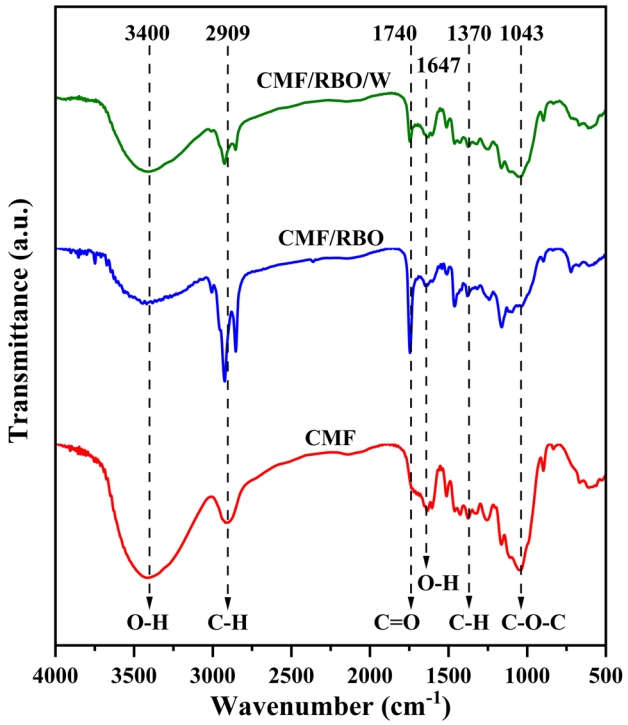

Fig. 11 FTIR spectra of cellulose fibers (CMF), chemically modified cellulose fibers (CMF/RBO), and chemically modified cellulose fibers after washing (CMF/RBO/W).

1740 cm^{-1}, characteristic of the C=O bond in the carbonyl group of esters. In addition, the FTIR spectrum of the cellulose sample after modification with RBO and subsequent washing three times with ethanol solution and five times with distilled water (CMF/RBO/W) exhibited absorption bands similar to those of the CMF/RBO sample. However, the absorption intensity of the peak at 1740 cm^{-1} in the CMF/RBO/W sample was lower than that of the CMF/RBO sample. This behavior was attributed to the washing process, which removed excess RBO that did not participate in the reaction. These results confirmed that the chemical modification treatment of cellulose fibers using RBO took place successfully. The reaction mechanism between cellulose fibers and Rice Bran Oil (RBO) was illustrated in Fig. S2 of the SI.

Energy dispersive X-ray spectroscopy (EDS)

Surface elemental mapping analysis based on EDS of unmodified cellulose fibers, rice bran oil (RBO)-modified cellulose fibers, and RBO-modified cellulose fibers after water washing is presented in Fig. 12. The analysis results showed that the carbon content of the RBO-modified cellulose fibers (69.8%) increased markedly compared to that of the unmodified cellulose fibers (49.9%), while the oxygen content exhibited a decreasing trend. This change indicated that surface modification with rice bran oil enriched the carbon content on the cellulose fiber surface and simultaneously reduced oxygen-containing functional groups. This phenomenon could be explained by an esterification reaction occurring between the

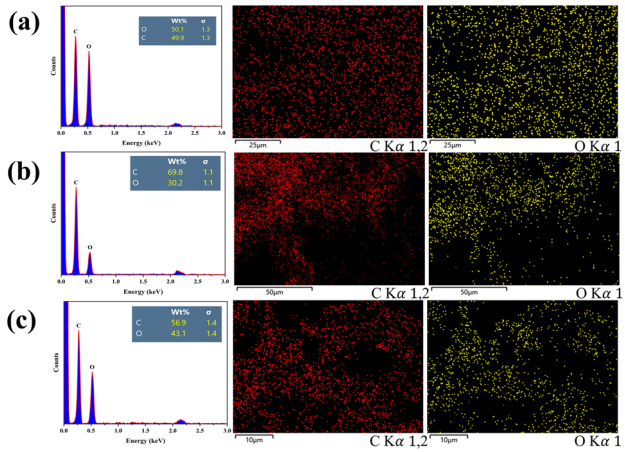

Fig. 12 EDS elemental mapping images of (a) cellulose fibers, (b) cellulose fibers after modification, and (c) modified cellulose fibers after washing.

hydroxyl groups of cellulose and the carboxyl groups present in rice bran oil, leading to the formation of ester linkages on the surface of the cellulose fibers. In addition, the RBO-modified cellulose fibers after water washing exhibited a relatively lower carbon content (56.9%) than that of the modified cellulose fibers prior to washing, but still higher than that of the unmodified cellulose fibers. This result could be attributed to repeated water washing, which removed unreacted rice bran oil coated on the surface of the cellulose fibers. These results confirmed that the surface modification of cellulose fibers with rice bran oil was successfully achieved.

Physicochemical properties of biocomposites based on PLA and cellulose fibers extracted from corn cobs

Surface morphology. The surface morphology of pristine PLA, biocomposites based on PLA and unmodified cellulose fibers (PLA/CMF), and biocomposites between PLA and RBO-modified cellulose fibers (PLA/RBO) were shown in Fig. 13. As

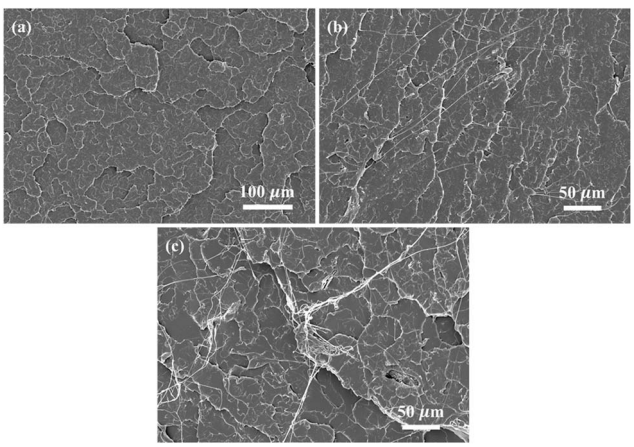

Fig. 13 SEM images of the fractured surfaces of the biocomposites after mechanical testing: (a) PLA; (b) PLA/RBO biocomposite; (c) PLA/CMF biocomposite.

observed from Fig. 13, the fractured surface of the PLA sample after mechanical testing shows a smooth texture. Besides that, all three samples exhibit grooves on their surfaces. Interestingly, the PLA/RBO sample reveals an unclear surface with unevenly distributed grooves. These grooves were formed due to the tensile forces applied during the mechanical testing process.[31]

Fig. 13c indicates that the micro-sized cellulose fiber agglomerations are presented with respect to PLA/CMF composite. This demonstrates the poor dispersion of unmodified cellulose fibers within the PLA matrix. This can be attributed to the incompatibility between hydrophilic cellulose fibers and hydrophobic PLA matrix. When the modified cellulose fibers were incorporated into the PLA matrix, an improvement in fiber dispersion within the PLA matrix was observed (Fig. 13b). Fiber agglomerations was significantly reduced, indicating better interfacial interaction between cellulose fibers and the PLA matrix.[40]

These results demonstrate that surface modification of cellulose fibers is essential for improving the compatibility between the cellulose fibers and PLA matrix.[41] The findings suggest that chemical modification treatment using RBO effectively reduced the polarity of cellulose fibers, facilitating their dispersion and adhesion within the PLA matrix.[25]

Crystalline structure of PLA and biocomposites. Fig. 14 and 15 shows the XRD patterns of pristine PLA, PLA/CMF, and PLA/RBO composites with different fiber contents. Pristine PLA exhibits four diffraction peaks at 16.40°, 18.88°, and 28.30°, corresponding to characteristic crystalline structures of PLA, which contains mainly amorphous structures.[42] Compared to those of pristine PLA, the XRD patterns of the PLA/CMF and PLA/RBO biocomposites show no new diffraction peaks. Therefore, the addition of 1–10 wt% of unmodified or chemically modified cellulose fibers did not change significantly the crystalline structures of PLA.[43]

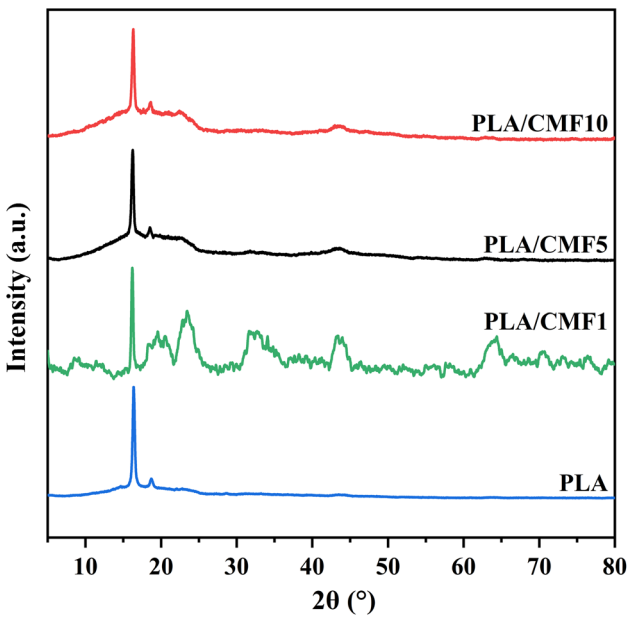

Fig. 14 XRD patterns of the PLA, PLA/CMF biocomposite with different fiber contents (1,5, and 10 wt%).

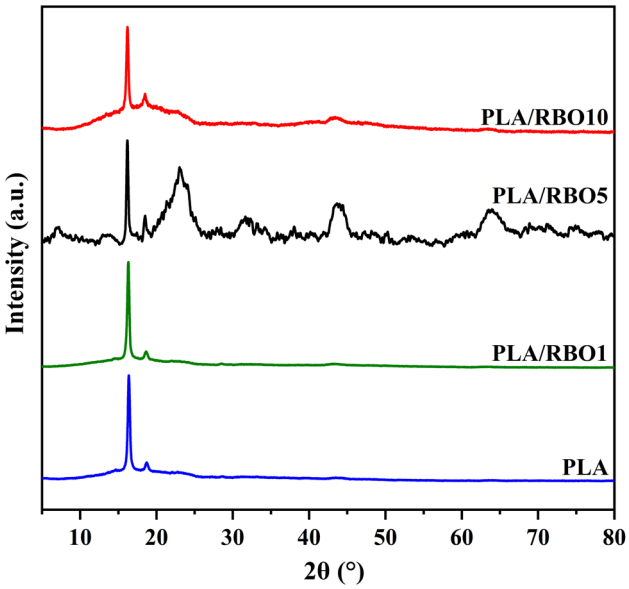

Fig. 15 XRD patterns of the PLA and PLA/RBO biocomposite with different fiber contents (1,5, and 10 wt%).

As can be seen from the Fig. 14 and Table 8, when the cellulose fiber content increased from 1 wt% to 10 wt%, the crystallinity index of the PLA/CMF biocomposites significantly decreased. This can be explained by the uneven dispersion of non-modified cellulose fibers in the PLA matrix, and the addition of too much non-modified cellulose fibers into the PLA matrix causing severe fiber agglomerations. These agglomerations act as obstacles, preventing the movement and arrangement of PLA chains. As a result, the crystallinity index of the biocomposites decreased significantly, leading to a reduction in mechanical strength.[44]

Furthermore, as observed from Fig. 15 and Table 8, the crystallinity index of PLA/RBO biocomposites was found to be higher than that of PLA/CMF biocomposites, especially for biocomposites with relatively low fiber contents (1 and 5 wt%). The PLA/RBO1 showed the highest crystallinity index of 26.2%, suggesting that the addition of 1 wt% cellulose fibers treated with RBO enhanced the crystallinity index of the biocomposite.

Table 8 Crystallinity index of PLA and PLA/CMF biocomposites with different fiber contents calculated using eqn (2)

Sample	Crystallinity index (%)
PLA	23.7
PLA/RBO1	26.2
PLA/CMF1	24.8
PLA/RBO5	25.3
PLA/CMF5	16.2
PLA/RBO10	14.2
PLA/CMF10	14.1

These results highlight the positive impact of surface modification of cellulose fibers on improving fiber-matrix interactions and promoting crystalline alignment.[45] Interestingly, as the fiber content increased to 5 wt% and 10 wt%, the CrI values decreased significantly for both biocomposites. These results indicate that higher fiber content potentially disrupts the crystalline order of the PLA matrix.

These findings suggest that while the incorporation of cellulose fibers, particularly those modified with RBO, can enhance the crystallinity of PLA biocomposites at low fiber content, excessive fiber loading negatively impacted crystallinity due to agglomeration and decreased compatibility.

From Fig. 16 and Table 8, it is shown that the addition of 1 wt% cellulose fiber to the PLA matrix increased the crystallinity index of the biocomposite compared to PLA. Notably, when 1 wt% of modified cellulose fibers were added to the PLA matrix, the crystallinity index of the biocomposite was enhanced more effectively than with 1 wt% of unmodified cellulose fibers. This indicates that the chemical modification process improved the interaction between cellulose fibers and the PLA matrix. These findings emphasize the importance of cellulose fiber content and the modification process in enhancing the crystallinity index of the biocomposites.[46]

Thermal properties of PLA/CMF biocomposites. Despite some favorable characteristics such as biodegradability and relatively high mechanical properties, PLA exhibits certain limitations, most notably a slow crystallization rate and a relatively low degree of crystallinity.[47] This sluggish crystallization behavior poses challenges in industrial processing. In this study, cellulose fibers were used as nucleating agents to improve the crystallization kinetics of the PLA matrix.

The non-isothermal crystallization behavior of PLA and biocomposites prepared by combining with 1 wt% unmodified cellulose fiber (PLA/CMF1) and 1 wt% RBO-modified cellulose fiber (PLA/RBO1) were investigated by DSC technique. DSC thermograms of PLA and biocomposites during the cooling scan cycle are presented in Fig. 17. As observed from Fig. 17, both PLA and PLA/CMF1 biocomposite did not show any melt crystallization peak upon cooling. Conversely, the melt crystallization peak (at around 98 °C) was observed for the PLA/RBO1 biocomposite material. This indicates that with addition of 1 wt% RBO-modified cellulose fiber helped induce the melt crystallization of PLA upon cooling. It is believed that RBO-modified cellulose fiber had good interfacial adhesion with PLA matrix. The well dispersed cellulose fibers within PLA matrix, acting as heterogeneous nucleating agents inducing the lower energy barrier required for the formation of crystal nuclei. This allows the melt crystallization upon cooling of PLA to take place.[48] This result is consistent with SEM result mentioned.

DSC thermograms of PLA and its biocomposites during the second heating scan are shown in Fig. 18. It was found that the cold crystallization temperature (the exothermic peaks at 99–102 °C) of the PLA/CMF1 biocomposite did not indicate any significant difference compared to that of PLA. This demonstrates that the addition of unmodified cellulose fiber into PLA matrix did not cause any change in crystallization rate of PLA. It is due to the incompatibility between relative polar cellulose fibers and nonpolar PLA matrix, leading to poor dispersion of fibers in PLA matrix. As a result, the unmodified cellulose fibers exhibited limited efficacy as nucleating agents and did not significantly enhance the crystallization rate of PLA. However, as observed from Fig. 18, the PLA/RBO1 biocomposite indicated a lower cold crystallization temperature compared to PLA and PLA/CMF1 biocomposite. This indicates that the addition of RBO-modified cellulose fiber induced the improvement in the crystallization rate of PLA. This result can be explained that the RBO-modified cellulose fiber dispersed well in PLA matrix allows the heterogeneous nucleation mechanism to occur. This induces a decrease of the free energy barrier and fastens the crystallization rate of PLA.[49] Besides that, it was found that the cold crystallization peak became broader for PLA/RBO1 biocomposite (Fig. 18).

Moreover, it can be seen from Fig. 18 that, with the addition of cellulose fibers, the glass transition temperatures (T_g) (the small endothermic peaks at around 55 °C) of PLA/CMF1 and

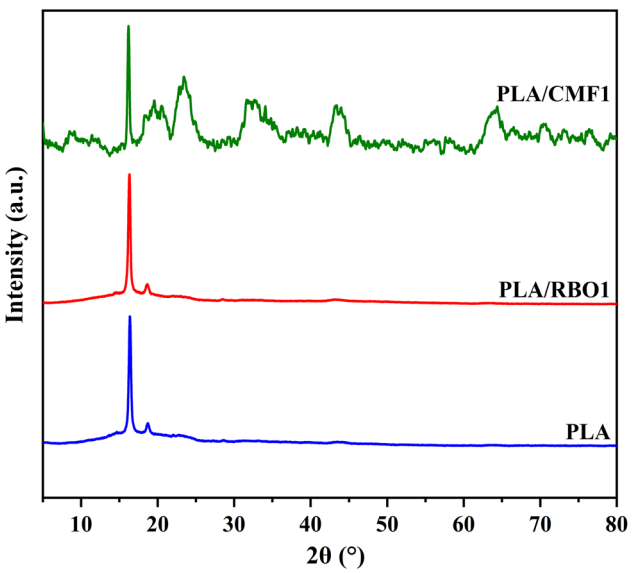

Fig. 16 XRD patterns of PLA, PLA/CMF1, and PLA/RBO1 samples.

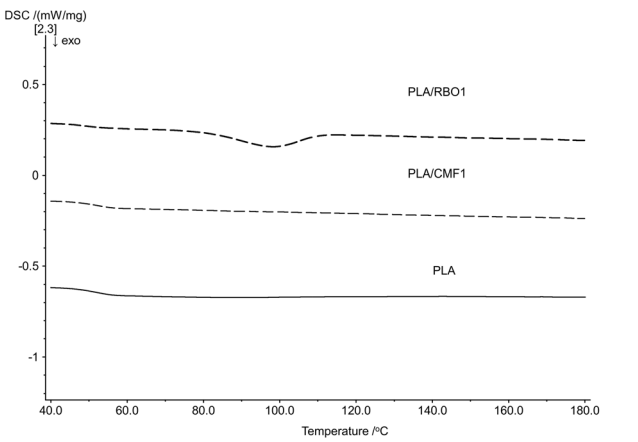

Fig. 17 DSC thermograms of PLA, PLA/CMF1, and PLA/RBO1 biocomposites (cooling cycle).

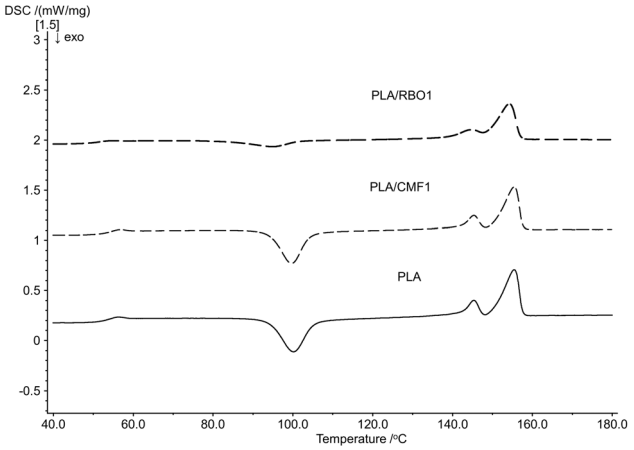

Fig. 18 DSC thermograms of PLA, PLA/CMF1, and PLA/RBO1 biocomposites (second heating cycle).

PLA/RBO1 biocomposites are slightly higher than that of PLA. This shift can be explained by the restriction of chain mobility with the presence of cellulose fibers.[50] Additionally, the RBO surface chemical modification of cellulose fiber was found to cause a slight decrease of the glass transition temperature in the case of PLA/RBO1 biocomposite.

Fig. 18 also shows that there are two melting temperatures (T_{m_1} (145 °C) and T_{m_2} (155 °C)) for both PLA and biocomposites. The lower melting temperature (T_{m_1}) is attributed to the melting of crystals formed during the cooling process from the melt, whereas the higher melting temperature (T_{m_2}) corresponds to the melting of more perfect crystals generated *via* cold crystallization upon subsequent heating.[51] As observed from Fig. 18, the melting temperatures (T_{m_1} and T_{m_2}) of PLA/CMF1 and PLA/RBO1 biocomposites did not show any significant difference compared to those of PLA.

Mechanical properties. It can be observed from Fig. 19 and 20 that the tensile strength of the PLA/RBO1 composite increased by approximately 2.38% compared to neat PLA, while the elongation at break and Young's modulus exhibited similar trends, increasing by 5.20% and 8.94%, respectively. These results indicated that the incorporation of 1 wt% surface-modified cellulose fibers enhanced interfacial interactions and fiber dispersion within the PLA matrix, thereby improving the overall mechanical performance of the biocomposite. In contrast, when the cellulose fiber content was increased from 5 wt% to 10 wt%, the PLA/RBO5 and PLA/RBO10 composites exhibited simultaneous reductions in tensile strength, elongation at break, and Young's modulus. This behavior was attributed to the excessive fiber loading, which restricts the mobility of PLA molecular chains and promotes fiber agglomeration, resulting in a non-homogeneous composite structure.[52] Overall, these findings demonstrated that an optimal cellulose fiber content of 1 wt% played a critical role in ensuring effective dispersion of surface-modified cellulose fibers within the PLA matrix, thereby maximizing the mechanical reinforcement efficiency of the composites.

From Fig. 21 and 22, it can be observed that the Young's modulus, tensile strength, and elongation at break of the PLA/CMF composites were all lower than those of neat PLA, indicating that the incorporation of unmodified cellulose fibers adversely affected the mechanical properties of the composites.[53] Specifically, when the cellulose fiber content increased from 1 wt% to 10 wt%, the elongation at break decreased markedly from 1.73 ± 0.16% to 0.99 ± 0.04%, reflecting a clear brittleness tendency of the material (Fig. 22b). This behavior can be attributed to the inherently rigid nature of cellulose fibers, combined with poor interfacial interactions, which lead to the formation of stress concentration points and non-uniform fiber dispersion within the PLA matrix, thereby creating structurally weak regions in the composite.[54–56] Meanwhile, the results in Fig. 22a showed that the tensile strength of PLA/CMF1, PLA/CMF5, and PLA/CMF10 decreased by approximately 49.1%, 37.4%, and 56.3%, respectively, compared to neat PLA, confirming that the insufficient interaction between

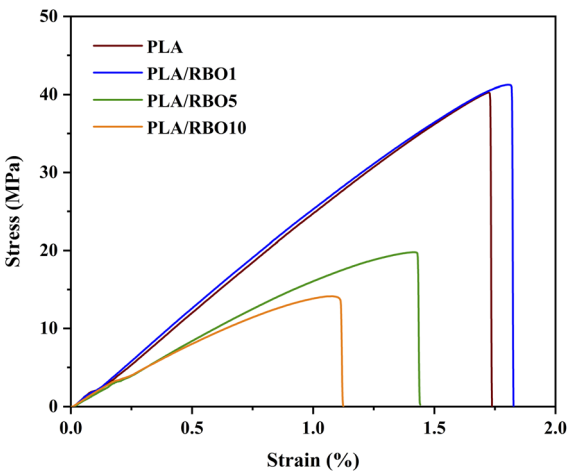

Fig. 19 Stress–strain curves of PLA, PLA/RBO samples with different fiber loadings.

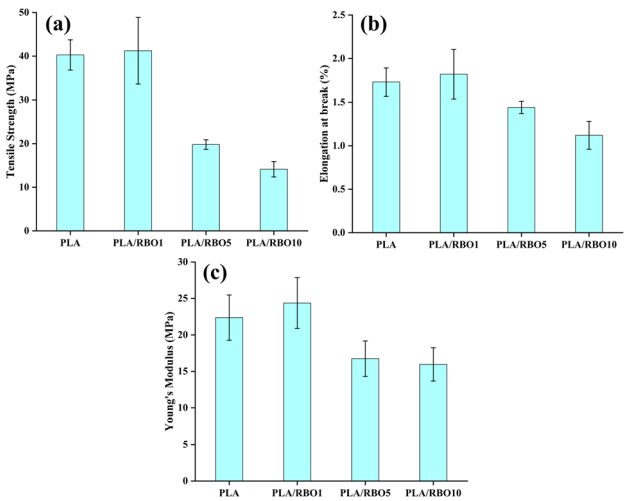

Fig. 20 (a) Tensile strength; (b) elongation at break; and (c) Young's Modulus of PLA and PLA/RBO1, PLA/RBO5, PLA/RBO10 biocomposites.

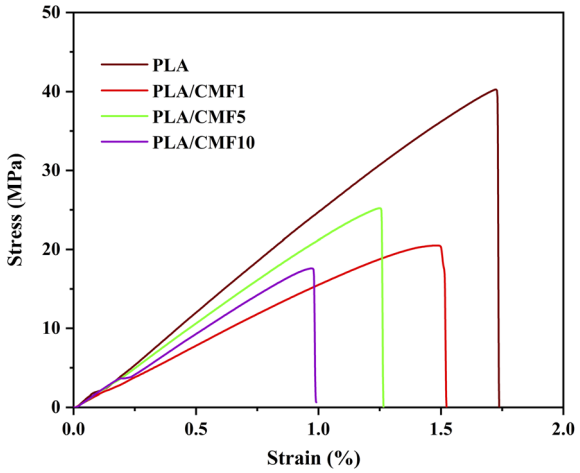

Fig. 21 Stress–strain curves of PLA, PLA/CMF samples with different fiber contents.

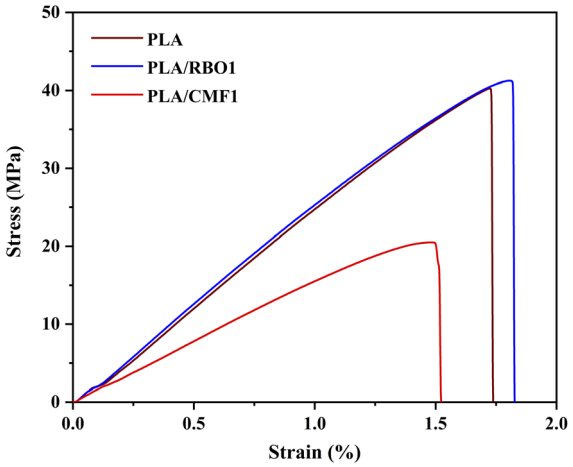

Fig. 23 Stress–strain curves of PLA, PLA/RBO1 and PLA/CMF1 samples.

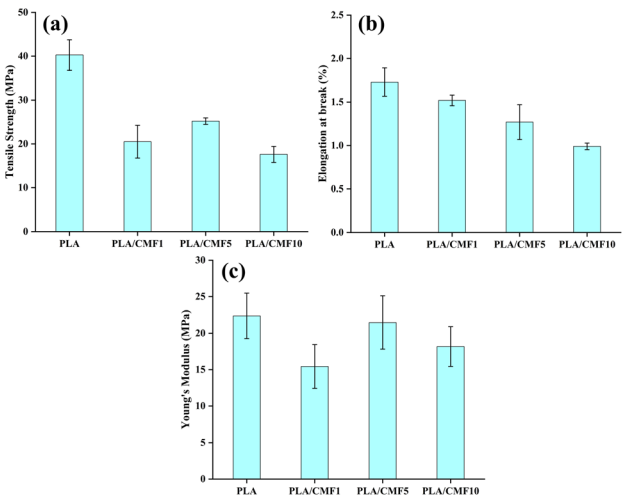

Fig. 22 (a) Tensile strength; (b) elongation at break; and (c) Young's modulus of PLA, PLA/CMF1, PLA/CMF5, and PLA/CMF10 biocomposites.

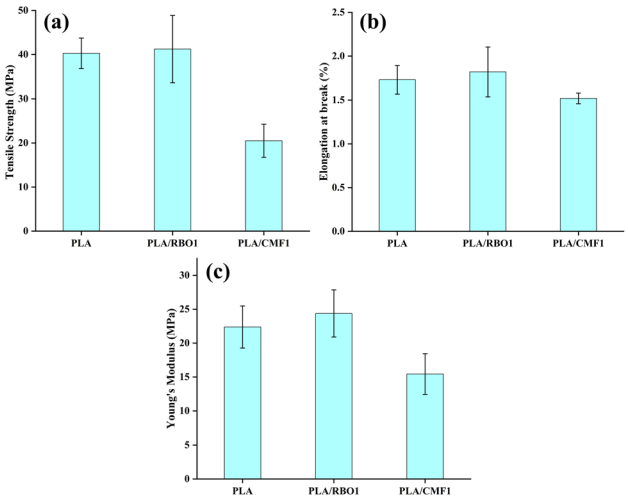

Fig. 24 Comparison of the mechanical properties of PLA, PLA/RBO1, and PLA/CMF1 biocomposites: (a) tensile strength; (b) elongation at break; and (c) Young's modulus.

cellulose fibers and the PLA matrix hindered effective stress transfer, and thus diminished the reinforcing role of the cellulose fiber.[53]

Based on the previous results, we selected the biocomposites with an optimal fiber content of 1 wt% for comparison with neat PLA. As shown in Fig. 23 and 24, the biocomposite containing 1 wt% surface-modified cellulose fibers exhibited higher tensile strength, elongation at break, and Young's modulus than both neat PLA and the composite reinforced with unmodified cellulose fibers. In contrast, the biocomposite containing unmodified cellulose fibers showed inferior mechanical properties, even lower than those of neat PLA. This pronounced difference demonstrated that cellulose surface modification played a decisive role in improving fiber–matrix compatibility, thereby enhancing stress transfer efficiency and suppressing premature failure. These findings clearly confirmed that the cellulose modification process was essential for achieving effective mechanical reinforcement in PLA-based biocomposites.[54,57] Table S4 of the SI summarizes the mechanical properties of biocomposite samples at different cellulose contents.

Rheological properties. Understanding the rheological properties of PLA/cellulose fibers biocomposites is vital for successful 3D printing. By optimizing these properties, it is possible to fabricate high-quality 3D products using PLA/cellulose fibers biocomposites as 3D filaments with enhanced mechanical performance. As reported from previous studies,[58–61] cellulose fibers, especially at higher loadings, tended to increase the melt viscosity of the biocomposites. This is due to the high surface area of the fibers and their tendency to form networks, hindering polymer chain mobility. The higher viscosity of PLA/cellulose fiber biocomposites affects layer adhesion, as the material may not flow and bond effectively. However, a certain level of viscosity of PLA/cellulose fiber

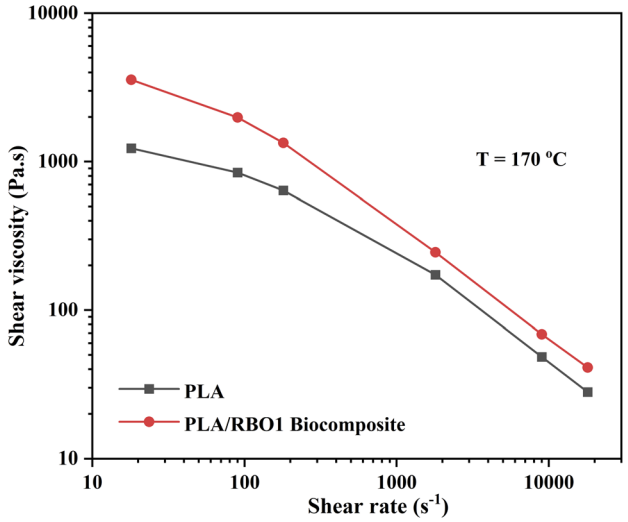

Fig. 25 Flow curves of PLA and PLA/RBO1 biocomposites.

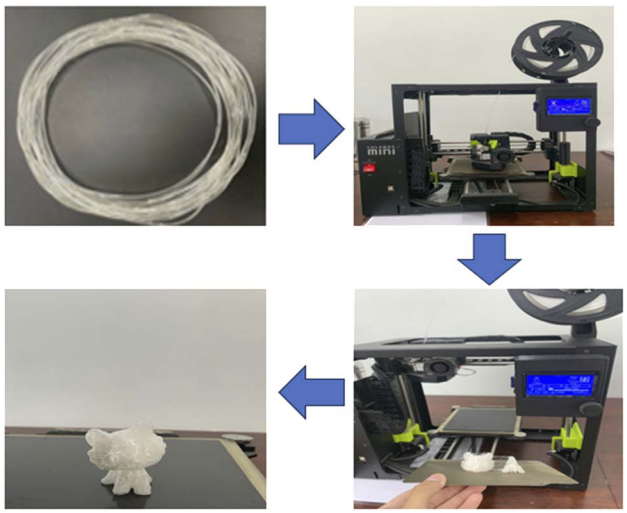

Fig. 26 3D printing process using the LulzBot Mini 2 3D printer.

Table 9 MFI values of PLA and PLA/RBO1 biocomposites at 170 °C

Sample	MFI (g/10 m)
PLA	2.72 ± 0.05
PLA/RBO1 biocomposite	2.58 ± 0.03

biocomposites is necessary to maintain filament shape and prevent sagging during 3D printing. Therefore, the determination of rheological properties of fabricated PLA/RBO1 biocomposites plays crucial role with regard to ability of using this material as environmentally friendly 3D printing material.

Flow curves of PLA and PLA/RBO1 biocomposites with cellulose fiber content of 1 wt% were shown in Fig. 25. It revealed that viscosity at all shear rate ranges of PLA/RBO1 biocomposite was higher than that of PLA. This is attributed to the lower molecular chain mobility of PLA due to the presence of cellulose fibers. Cellulose fibers served as physical crosslinking points. As a result, the higher viscosity of PLA/RBO1 biocomposites was obtained. This result is in good agreement with MFI result as presented in Table 9. PLA/RBO1 biocomposites showed lower MFI than PLA, indicating the higher viscosity. These results indicate that after chemical modification, the interfacial adhesion between cellulose fibers and PLA matrix was improved, which led to lowering the PLA chain flexibility and higher shear viscosity of PLA/RBO1 biocomposites compared to that of PLA at all measured shear rates. In addition, the rheological properties of the biocomposites reinforced with different cellulose contents are presented in Fig. S3 of the SI.

Evaluation of the applicability of PLA/CMF biocomposite as 3D printing material using fused deposition modelling technology

The PLA/RBO1 biocomposite was used to fabricate filaments with a diameter of 1.72 ± 0.06 mm and was subsequently employed as a 3D printing material. The parameters and procedural steps of the 3D printing process were presented in Table S5 and Fig. 26, respectively.

Dimensional accuracy

The dimensional accuracy of the 3D-printed specimens was evaluated based on the thickness, width at the gauge length region, and overall length of the samples, in accordance with ASTM D638 Type IV. The design drawing following the ASTM D638 Type IV standard was presented in Fig. S4. In fused deposition modeling (FDM) 3D printing, the actual dimensions of printed parts often deviated from the original design dimensions due to thermal shrinkage and process-related factors. According to previous studies, the dimensional deviation of FDM-printed samples typically ranged from 0.1 to 1.4%, corresponding to the shrinkage behavior of thermoplastic polymers during printing and cooling.[26] The average dimensions and dimensional deviations of the 3D-printed samples were summarized in Table 10. The results showed that both material systems exhibited dimensional deviations below 3%. For the width and thickness dimensions, the neat PLA samples exhibited larger dimensional deviations than the PLA/RBO1 samples. This behavior was attributed to the reinforcement effect of cellulose microfibers modified with rice bran oil, which reduced the mobility of PLA chains, thereby limiting filament spreading after extrusion and stabilizing the molten flow during printing.[62] In addition, the presence of cellulose acted as physical crosslinking points within the polymer matrix, increasing the viscosity and stiffness of the PLA/RBO1 system compared with neat PLA. This effect contributed to reduced thermal shrinkage and improved dimensional accuracy of the printed samples.[63] For the specimen length, the results indicated that neat PLA exhibited a smaller length deviation than PLA/RBO1. This behavior was attributed to the lower melt viscosity of neat PLA, which led to stronger polymer chain orientation along the printing direction. In contrast, the

Table 10 Mean dimensions and dimensional deviations of the 3D-printed specimens

Sample	Width (mm)	Deviation (%)	Length (mm)	Deviation (%)	Thickness (mm)	Deviation (%)
PLA	5.90 ± 0.01	1.67	114.86 ± 0.13	0.12	3.11 ± 0.06	2.88
PLA/RBO1 biocomposite	5.94 ± 0.11	0.97	114.59 ± 0.11	0.36	3.19 ± 0.02	0.31

presence of CMF restricted chain orientation, resulting in more uniform shrinkage in different directions and improved overall geometric stability of the composite material. However, dimensional accuracy in FDM printing depended on multiple processing parameters; therefore, a more in-depth discussion of this issue is required.

In addition, a preliminary evaluation of the mechanical properties of the 3D-printed samples was presented in Fig. S5 of the SI.

Limitations and future development

Limitations. Although biocomposite materials based on poly(lactic acid) (PLA) and cellulose fibers derived from agricultural waste corn cobs have demonstrated potential as environmentally friendly materials for 3D printing applications, this study still exhibits several limitations that should be addressed in future research. First, the chemical extraction process used to obtain cellulose microfibers consumes a large amount of chemicals and requires extensive water usage during the washing steps to remove residual reagents, resulting in significant water and energy consumption. Second, the reinforcing efficiency as well as the maximum loading content of cellulose microfibers in the PLA matrix remain relatively low, thereby limiting the extent of mechanical property enhancement of the biocomposite.

Furthermore, the interfacial interactions between rice bran oil (RBO)-modified cellulose microfibers and the PLA matrix have only been qualitatively evaluated based on SEM, FTIR, and XRD analyses, while quantitative assessments of interfacial adhesion have not yet been conducted. In addition, a life cycle assessment (LCA) of the fabricated biocomposite has not been performed, although this analysis is essential for evaluating its practical applicability and sustainability. Finally, although the feasibility of the biocomposite as a 3D printing material for fused deposition modeling (FDM) technology has been demonstrated, key printing parameters—such as dimensional accuracy, interlayer adhesion, and the mechanical properties of the final printed parts-have not yet been systematically investigated.

Future development. Future research on bio-based composite filaments derived from poly(lactic acid) (PLA) and cellulose microfibers obtained from agricultural waste should place greater emphasis on industrial scalability and practical implementation. First, cellulose extraction processes should be further optimized toward greener, low-energy, and scalable approaches. Alternative pretreatment methods, such as enzymatic treatment, deep eutectic solvents, or hybrid mechanical–chemical processes, may be explored to reduce chemical consumption, processing time, and environmental impact while maintaining sufficient fiber quality for effective reinforcement in filament production. In addition, other agricultural waste resources should be investigated to further mitigate agricultural waste generation in Vietnam.

Moreover, systematic studies on surface modification strategies for cellulose microfibers are required to reduce hydrophilicity, enhance dispersion, and improve interfacial compatibility with the PLA matrix. Beyond rice bran oil (RBO), other bio-based modification agents or compatibilizers may be examined to enhance mechanical performance without compromising processability or the quality of printed parts.

Subsequent investigations should also focus on elucidating the relationships among filament extrusion parameters, FDM printing conditions, and the resulting microstructure and mechanical anisotropy of printed components. The integration of rheological modeling with real-time process monitoring may provide deeper insights into melt-flow behavior and interlayer bonding mechanisms, thereby enabling the development of optimized printing protocols for bio-composite materials.

In addition to tensile properties, mechanical characterization should be extended to include flexural strength, impact resistance, and environmental aging behavior under exposure to humidity, heat, and UV radiation in order to assess material suitability for real-world applications. Concurrently, studies on controlled biodegradation under different environmental conditions would yield critical information regarding the end-of-life phase of the printed products.

Finally, life cycle assessment (LCA), recyclability, and integration into circular economy models should be emphasized to clarify the feasibility of reprocessing and reusing printed PLA/cellulose components. Collectively, these research directions will facilitate the transition of bio-based composite materials from laboratory-scale development to environmentally sustainable commercial 3D-printing applications.

Conclusions

The findings of this study have demonstrated the potential of cellulose fibers extracted from corn cobs – an agricultural waste source for fabricating sustainable biocomposite materials using biodegradable poly(lactic acid) as the matrix. The extraction process employed optimal conditions and environmentally friendly extraction methods, using non-toxic chemicals. The use of H_2O_2 and NaOH was highly effective in removing impurities while preserving the structure and characteristic properties of cellulose fibers. Besides that, H_2O_2 also functioned as a bleaching agent, effectively removed most of the hemicellulose and lignin components from the fiber structure.

Additionally, the surface chemical modification of cellulose fibers using rice bran oil (RBO) significantly improved the compatibility between the cellulose fibers and the PLA matrix. This chemical modification reduced the polarity of the cellulose fibers without harming the environment due to using an environmentally friendly organic acid RBO. The results of FTIR, XRD, SEM, TGA, DSC analyses in combination with rheological and mechanical characterizations provided critical insights into the structure and physicochemical properties of the fabricated biocomposites based on cellulose fibers and poly(lactic acid), particularly its enhanced crystallinity and mechanical performance.

With a cellulose fiber content of 1 wt%, the biocomposites obtained optimal mechanical properties with improved tensile strength, elongation at break, and elastic modulus. The 3D printing process by FDM method using the filament fabricated from PLA and cellulose fibers extracted from corn cobs agricultural waste demonstrated its feasibility for application as 3D printing material. The successful development of biocomposites from renewable resources not only paves the way for the production of biodegradable products but also addresses environmental challenges, aligning with the goal of sustainable development of Vietnam in the future.

Author contributions

Nguyen Chi Thanh: conceptualization, data curation, formal analysis, investigation, methodology, supervision, validation, visualization, writing – original draft, writing – review& editing. Pham Duc Thinh: data curation, formal analysis, investigation, visualization, writing – original draft, writing – review & editing. Bui Phuong Dong: formal analysis, writing – review & editing. Tran Hai Cat: formal analysis, writing – review & editing. Nguyen Thanh Huy: formal analysis, writing – review & editing.

Conflicts of interest

There are no conflicts to declare.

Data availability

The supporting data has been provided as part of the supplementary information (SI). Supplementary information is available. See DOI: https://doi.org/10.1039/d5ra09705c.

Acknowledgements

The authors would like to thank Ho Chi Minh City University of Technology and Engineering for the financial support. This study belongs to the project grant No: T2026-35.

References

1 H. A. Silvério, W. P. F. Neto, N. O. Dantas and D. Pasquini, *Ind. Crop. Prod.*, 2013, **44**, 427–436.
2 W. K. Ng, W. S. Chow and H. Ismail, *Polym. Renew. Resour.*, 2019, **10**, 63–76.
3 U. N. Ngoc and H. Schnitzer, *Waste Manag.*, 2009, **29**, 1982–1995.
4 T. M. Vu, D. P. Doan, H. T. Van, T. V. Nguyen, S. Vigneswaran and H. H. Ngo, *Sci. Total Environ.*, 2017, **579**, 612–619.
5 Y. Zou, J. Fu, Z. Chen and L. Ren, *Agriculture*, 2021, **11**, 556.
6 R. S. Abolore, S. Jaiswal and A. K. Jaiswal, *Carbohydr. Polym. Technol. Appl.*, 2024, **7**, 100396.
7 L. Chopra, *Mater. Today: Proc.*, 2022, **48**, 1265–1270.
8 M. P. Menon, R. Selvakumar and S. Ramakrishna, *RSC Adv.*, 2017, **7**, 42750–42773.
9 A. N. Frone, D. M. Panaitescu and D. Donescu, *Sci. Bull. - "Politeh." Univ. Bucharest, Ser. B*, 2011, **73**, 133–152.
10 J. Wang, R. Zhang, C. Quan, X. Shao, N. Hu, X. Yao and C. Dong, *Cellulose*, 2022, **29**, 7125–7138.
11 H. Chen, Y. Yuan and Q. Li, *Starch-Stärke*, 2020, **72**, 1900209.
12 A. Fouly, A. K. Assaifan, I. A. Alnaser, O. A. Hussein and H. S. Abdo, *Polymers*, 2022, **14**, 5299.
13 S. Farah, D. G. Anderson and R. Langer, *Adv. Drug Deliv. Rev.*, 2016, **107**, 367–392.
14 H. Ramezani Dana and F. Ebrahimi, *Polym. Eng. Sci.*, 2023, **63**, 22–43.
15 C. A. Murphy and M. N. Collins, *Polym. Compos.*, 2018, **39**, 1311–1320.
16 X. Pang, X. Zhuang, Z. Tang and X. Chen, *Biotechnol. J.*, 2010, **5**, 1125–1136.
17 N. G. Khouri, J. O. Bahú, C. Blanco-Llamero, P. Severino, V. O. C. Concha and E. B. Souto, *J. Mol. Struct.*, 2024, 138243.
18 V. G. Gorade, A. Kotwal, B. U. Chaudhary and R. D. Kale, *J. Polym. Res.*, 2019, **26**, 1–12.
19 X. Bi and R. Huang, *Mater. Des.*, 2022, **222**, 111065.
20 A. Ji, S. Zhang, S. Bhagia, C. G. Yoo and A. J. Ragauskas, *RSC Adv.*, 2020, **10**, 21698–21723.
21 B. B. Mansingh, J. S. Binoj, Z. Q. Tan, W. W. L. Eugene, T. Amornsakchai, S. A. Hassan and K. L. Goh, *Polym. Compos.*, 2022, **43**, 6051–6061.
22 V. H. M. D. Almeida, R. M. D. Jesus, G. M. Santana, S. Khan, E. F. M. S. Silva, I. S. D. Cruz, I. D. S. Santos and P. N. M. Dos Anjos, *Polymers*, 2024, **16**, 1757.
23 S. Raja, R. M. Ali, S. Karthikeyan, R. Surakasi, R. Anand, N. Devarasu and T. Sathish, *Chem. Eng.*, 2024, **7**, 10–59429.
24 L. Segal, J. Creely, Jr., A. E. Martin Jr and C. M. Conrad, *Textil. Res. J.*, 1959, **29**, 786–794.
25 H. Li, Z. Cao, D. Wu, G. Tao, W. Zhong, H. Zhu, P. Qiu and C. Liu, *Plast., Rubber Compos.*, 2016, **45**, 181–187.
26 W. Prasong, A. Ishigami, S. Thumsorn, T. Kurose and H. Ito, *Polymers*, 2021, **13**, 740.
27 A. El Oudiani, Y. Chaabouni, S. Msahli and F. Sakli, *Carbohydr. Polym.*, 2011, **86**, 1221–1229.
28 Z. Wang, A. G. McDonald, R. J. M. Westerhof, S. R. A. Kersten, C. M. Cuba-Torres, S. Ha, B. Pecha and M. Garcia-Perez, *J. Anal. Appl. Pyrolysis*, 2013, **100**, 56–66.
29 R. D. Kale, P. S. Bansal and V. G. Gorade, *J. Polym. Environ.*, 2018, **26**, 355–364.
30 G. Maschio, C. Koufopanos and A. Lucchesi, *Bioresour. Technol.*, 1992, **42**, 219–231.
31 H. Gao and T. Qiang, *Materials*, 2017, **10**, 624.

32 Y. Su, R. Du, H. Guo, M. Cao, Q. Wu, R. Su, W. Qi and Z. He, *Food Bioprod. Process.*, 2015, **94**, 322–330.
33 Y. H. P. Zhang, *J. Ind. Microbiol. Biotechnol.*, 2008, **35**, 367–375.
34 X. F. Sun, F. Xu, R. C. Sun, P. Fowler and M. S. Baird, *Carbohydr. Res.*, 2005, **340**, 97–106.
35 H. Du, K. Liu, T. Xu, C. Xu, M. Lin, Z. Fang, S.-W. Kim, J.-Y. Seo, J. Chen, H. Ma, B. S. Hsiao, L. W. DeVetter, Z. Piao, C. Si, C. Chen, Q. Yang, S.-Y. Lee, Y. Yao and X. Pan, *Chem. Rev.*, 2025, **125**, 11666–11814.
36 K. Kaur, R. Kaur and H. Kaur, *Appl. Surf. Sci. Adv.*, 2024, **19**, 100547.
37 Y. Zhan, X. Liu, C. Huang, X. Zhou, Y. Lyu, Y. Lin, C. Huang, W. Ma, Z. Xie, G. Fang and A. J. Ragauskas, *Ind. Crops Prod.*, 2024, **214**, 118533.
38 M. J. Selig, T. B. Vinzant, M. E. Himmel and S. R. Decker, *Appl. Biochem. Biotechnol.*, 2009, **155**, 94–103.
39 K. O. Reddy, J. Zhang, J. Zhang and A. V. Rajulu, *Carbohydr. Polym.*, 2014, **114**, 537–545.
40 S. Qian, H. Zhang, W. Yao and K. Sheng, *Composites, Part B*, 2018, **133**, 203–209.
41 M. R. Manshor, H. Anuar, M. N. N. Aimi, M. I. A. Fitrie, W. B. W. Nazri, S. M. Sapuan, Y. A. El-Shekeil and M. U. Wahit, *Mater. Des.*, 2014, **59**, 279–286.
42 T. Lu, M. Jiang, X. Xu, S. Zhang, D. Hui, J. Gou and Z. Zhou, *J. Appl. Polym. Sci.*, 2014, **131**, 41077.
43 D. Wu, L. Wu, L. Wu, B. I. N. Xu, Y. Zhang and M. Zhang, *J. Polym. Sci., Part B: Polym. Phys.*, 2007, **45**, 1100–1113.
44 A. Pei, Q. Zhou and L. A. Berglund, *Compos. Sci. Technol.*, 2010, **70**, 815–821.
45 M. Mohammed, R. Rahman, A. M. Mohammed, T. Adam, B. O. Betar, A. F. Osman and O. S. Dahham, *Polym. Test.*, 2022, **115**, 107707.
46 T. Lu, S. Liu, M. Jiang, X. Xu, Y. Wang, Z. Wang, J. Gou, D. Hui and Z. Zhou, *Composites, Part B*, 2014, **62**, 191–197.
47 S. S. Shazleen, L. Y. Foong Ng, N. A. Ibrahim, M. A. Hassan and H. Ariffin, *Polymers*, 2021, **13**, 3226.
48 S. S. Shazleen, T. A. T. Yasim-Anuar, N. A. Ibrahim, M. A. Hassan and H. Ariffin, *Polymers*, 2021, **13**, 389.
49 K. Shi, G. Liu, H. Sun, B. Yang and Y. Weng, *Polymers*, 2022, **14**, 4305.
50 V. de Oliveira, L. N. Horiuchi, A. P. Goncalves, M. De Andrade and R. Polkowski, Nanocomposites Made with Poly (Lactic Acid)/Cellulose Nanofibers for Automotive Applications: The Impact of Annealing on 3D Printed Parts, *Report 0148-7191, SAE Technical Paper*, 2025.
51 Y. Hu, H. Shen, H. Ni, Y. Liu, L. Zhang and G. Ju, *J. Appl. Polym. Sci.*, 2025, e56796.
52 T. Lu, M. Jiang, Z. Jiang, D. Hui, Z. Wang and Z. Zhou, *Composites, Part B*, 2013, **51**, 28–34.
53 L. Suryanegara, A. N. Nakagaito and H. Yano, *Cellulose*, 2010, **17**, 771–778.
54 A. N. Frone, S. Berlioz, J. F. Chailan, D. M. Panaitescu and D. Donescu, *Polym. Compos.*, 2011, **32**, 976–985.
55 M. E. Lozano Fernandez and N. Miskolczi, *Polymers*, 2022, **14**, 1887.
56 N. Graupner, *J. Mater. Sci.*, 2008, **43**, 5222–5229.
57 A. K. Trivedi, M. K. Gupta and H. Singh, *Adv. Ind. Eng. Polym. Res.*, 2023, **6**, 382–395.
58 K. Badura and P. Bazan, *Int. J. Adv. Res. Sci. Commun. Technol.*, 2025, **19**, 184–201.
59 N. J. Hadi, T. Rydzkowski, Z. S. Ali and Q. A. Al-Jarwany, *Coatings*, 2025, **15**, 397.
60 M. Lecoublet, M. Ragoubi, N. Leblanc and A. Koubaa, in *Sustainable Nanocomposites with Green Biomaterials*, Springer, 2025, pp. 445–477.
61 S. Antony Jose, N. Cowan, M. Davidson, G. Godina, I. Smith, J. Xin and P. L. Menezes, *Nanomaterials*, 2025, **15**, 356.
62 M. Lecoublet, M. Ragoubi, N. Leblanc and A. Koubaa, *Ind. Crops Prod.*, 2024, **221**, 119332.
63 F. Burkhardt, V. D. Schmidt, C. Wesemann, C. G. Schirmeister, S. Rothlauf, S. Pieralli, L. S. Brandenburg, L. Kleinvogel, K. Vach and B. C. Spies, *Sci. Rep.*, 2022, **12**, 20341.